Journal of Engineering Mathematics **30:** 661–682, 1996.

The scattering of water waves by an array of circular cylinders in a channel

C.M. LINTON and P. McIVER
Department of Mathematical Sciences, Loughborough University, Leicestershire LE11 3TU, UK

Received 20 June 1994; accepted in revised form 30 November 1995

Key words: scattering, cylinders, water waves, channel, multipoles

Abstract. The full linear problem of the scattering of water waves by an array of N bottom-mounted vertical circular cylinders situated in a channel of constant depth and width is solved using the method of multipoles. A simple formula is derived for the velocity potential in the vicinity of a cylinder, and in particular on the cylinder surfaces, which allows hydrodynamic quantities such as forces to be easily evaluated. The simplicity of the solution makes the evaluation of quantities of interest straightforward and extensive results are given. An approximate solution for the forces on the cylinders, based on the assumption that the wavelength of the incident wave is long compared with the cylinder radii, is also given, and this is compared with results from the 'exact' linear solution.

1. Introduction

Experiments to determine the hydrodynamic forces on offshore structures are often performed in wave tanks and the results used as approximations to the open-sea values. No matter how wide the tank is, it is clearly important to have a good understanding of how the tank walls affect the results of such experiments, and a number of recent papers have addressed this question.

One approach is to consider the problem for certain special geometries for which some analytic progress can be made. Thus, Eatock Taylor and Hung [1], Yeung and Sphaier [2, 3] and Thomas [4] used the method of images to solve linear radiation and scattering problems for a vertical circular cylinder in a channel, in some cases extending throughout the entire fluid depth and in others truncated. Linton and Evans [5] and McIver and Bennett [6], hereafter referred to as I and II, respectively, showed how the use of a multipole method facilitates the solution of such problems. The use of multipoles also enabled the existence of the phenomenon of trapped modes near bodies in channels, previously undiscovered in the water wave context, to be proved (see Callan, Linton and Evans [7]).

Many offshore structures, however, consist of not one, but a number of vertical cylindrical components and it is the purpose of this paper to investigate the hydrodynamic characteristics of such an array when it is considered fixed in the confines of a channel and in the presence of an incident plane wave.

Five papers have been published recently in which problems connected with the interaction of waves and arrays of vertical circular cylinders are solved numerically. Bharatkumar, Mahadevan and Pranesh [8] used a Green's function approach together with the method of images to obtain an integral equation and thus compute pressures and first-order forces on pairs of vertical circular cylinders in a channel. The same approach was used by Butler and Thomas [9] who also computed reflection and transmission coefficients and by Neelamani,

Bharatkumar, Mahadevan and Sundar [10] who compared results for a particular two-cylinder geometry with those from experiments. A more sophisticated technique was employed by Kashiwagi [11] who constructed a fully three-dimensional Green's function which automatically satisfied the channel-wall boundary conditions, thus eliminating the need to sum over all the image cylinders. Kashiwagi also presented results for the realistic case of four truncated cylinders arranged in a square, computed mean second-order drift forces and compared his results with experimental data. Mean drift loads on arrays of two and four cylinders extending throughout the water depth were also considered by Williams and Vazquez [12] using a similar method.

In all the above cases the theory is applicable to cylinders of arbitrary cross-section, although results are only shown for the circular case. For general-shaped obstacles this technique is extremely useful, but its implementation is quite difficult owing to the numerical problems that arise. It is well known that, when the method of images is used, the evaluation of the Green's function is complicated by the need to evaluate slowly convergent series of Hankel functions and different authors have used different methods to deal with this problem. A particularly efficient technique is described in Yeung and Sphaier [2]. The use of a more sophisticated Green's function is preferable, though only if a representation can be found that is straightforward to compute. The forms for the fully three-dimensional Green's function used by Kashiwagi [11] and for the two-dimensional case by Williams and Vazquez [12] both have their limitations. In [11] the numerical evaluation of a double integral is required, whilst in [12] the singular part of the Green's function does not appear explicitly, making accurate calculations difficult. Alternative forms for these fundamental solutions that may provide for more efficient computations have been derived in Linton [13] and Linton and Evans [14], respectively.

For the case of circular cylinders, however, another technique is available, that of multipole expansions, and this approach will be pursued here. The solution of the problem of scattering by an array of cylinders in a channel is found by combining the method of Linton and Evans [15] where the open-sea diffraction problem was solved, and techniques described in I and II where the problem of scattering by a single cylinder in a channel was solved. The resulting procedure is both fast and accurate and can be used to validate more general numerical codes as well as produce extensive results for hydrodynamic characteristics in this interesting problem.

The plan of the paper is as follows. In Section 2 the multipole method is formulated, formulas for the multipoles themselves being given in the Appendix. A simple formula for the velocity potential in the vicinity of a particular cylinder is derived which leads to straightforward expressions for the first-order and mean second-order forces on the cylinders. Another advantage of the multipole technique is the fact that the far-field form of the solution can be obtained explicitly. This results in simple expressions for the reflection and transmission coefficients as well as formulas which can be used as checks to validate the results. In Section 3 an approximate solution based on the assumption that the wavelength of the incident wave is large compared to the cylinder radii is derived using matched asymptotic expansions. This is an extension of work on the single cylinder case given in II. Extensive results are then given in Section 4.

2. Multipole Formulation

Cartesian coordinates (x, y, z) are chosen with z vertically upwards, $z = -h$ being the bottom of the channel and $z = 0$ the mean free surface. The channel has width $2d$ with the walls given

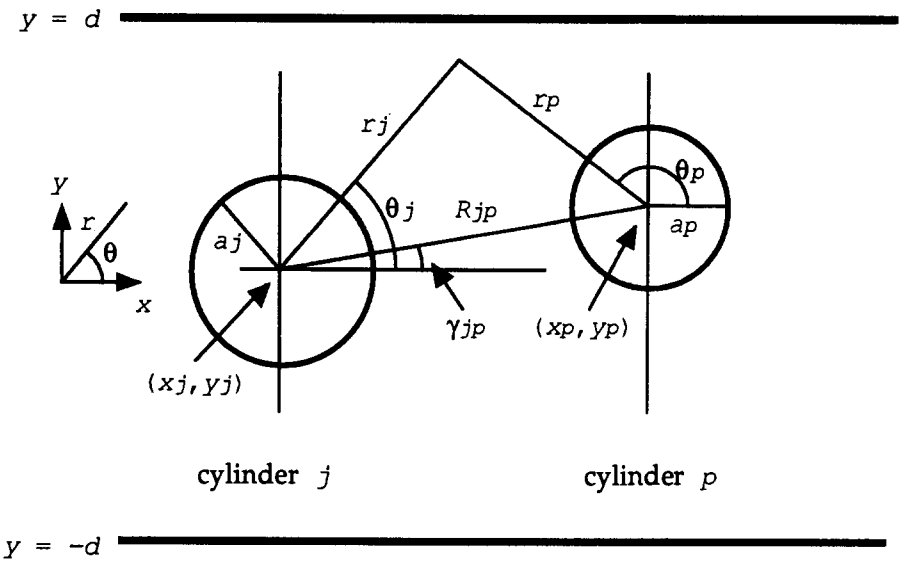

Figure 1. Plan view of two cylinders.

by the planes $y = \pm d$. We assume that there are $N(\geq 1)$ fixed vertical circular cylinders and use $N + 1$ polar coordinate systems in the (x, y)-plane: (r, θ) are centred at the origin, whilst (r_j, θ_j), $j = 1, \ldots, N$, are centred at (x_j, y_j), the centre of the jth cylinder. The various parameters relating to the relative positions and sizes of the cylinders are shown in Figure 1.

Under the usual assumptions of linear water-wave theory for time-harmonic motion with angular frequency ω we write

$$\Phi = \mathrm{Re}\{\phi(x, y) f(z) \mathrm{e}^{-\mathrm{i}\omega t}\}, \tag{2.1}$$

where

$$f(z) = -\frac{\mathrm{i}gA \cosh k(z + h)}{\omega \cosh kh} \tag{2.2}$$

and the wavenumber k is the real positive solution of the dispersion relation

$$k \tanh kh = \omega^2/g. \tag{2.3}$$

The two-dimensional potential ϕ then satisfies the Helmholtz equation

$$(\nabla^2 + k^2)\phi = 0. \tag{2.4}$$

We will assume the presence of an incident plane wave of amplitude A from $x = -\infty$ characterized by $\phi_I(x, y)$ where

$$\phi_I = \mathrm{e}^{\mathrm{i}kx} = \mathrm{e}^{\mathrm{i}kr\cos\theta}. \tag{2.5}$$

If we define a phase factor for each cylinder, I_j, by

$$I_j = \mathrm{e}^{\mathrm{i}kx_j}, \tag{2.6}$$

then we can write

$$\phi_I = I_j \mathrm{e}^{\mathrm{i}kr_j\cos\theta_j} = I_j \sum_{m=0}^{\infty} \epsilon_m \mathrm{e}^{\mathrm{i}m\pi/2} J_m(kr_j) \cos m\theta_j. \tag{2.7}$$

(Abramowitz and Stegun [16], equations (9.1.44) and (9.1.45)). Here $\epsilon_0 = 1$, whereas $\epsilon_n = 2$, $n \geq 1$.

The idea behind the multipole method is to construct functions (which will be denoted by ϕ_n^j, ψ_n^j) that are singular at (x_j, y_j) and satisfy (2.4), together with the wall boundary conditions and an appropriate radiation condition. Here the index n refers to the order of the multipole, whereas the index j refers to the number of the cylinder. Expressions for these multipoles are given in the Appendix and a number of useful properties of such functions are derived. We then write

$$\phi = \phi_I + \sum_{j=1}^{N} \sum_{n=0}^{\infty} Z_n^j (A_n^j \phi_n^j + B_n^j \psi_n^j), \tag{2.8}$$

where, for convenience, the factor $Z_n^j = J_n'(ka_j)/H_n'(ka_j)$ is introduced, H_n is used to denote the Hankel function $H_n^{(1)}$, and B_0^j is assumed to be zero, but is retained in the analysis. In what follows the scaled variables given by

$$\tilde{A}_n^j = Z_n^j A_n^j, \quad \tilde{B}_n^j = Z_n^j B_n^j \tag{2.9}$$

will also be used.

In order to apply the boundary condition on the cylinder surfaces, which is

$$\frac{\partial \phi}{\partial r_p} = 0 \quad \text{on } r_p = a_p, \quad p = 1, \ldots, N, \tag{2.10}$$

equation (2.8) must be written solely in terms of the coordinates r_p and θ_p. This is accomplished using the polar coordinate expansions of the multipoles, (A.1), (A.2), (A.14) and (A.15). We can thus write

$$\begin{aligned}
\phi = \sum_{n=0}^{\infty} \Big\{ & I_p \epsilon_m \, \mathrm{e}^{\mathrm{i}m\pi/2} J_m(kr_p) \cos m\theta_p + H_m(kr_p)(\tilde{A}_m^p \cos m\theta_p + \tilde{B}_m^p \sin m\theta_p) \\
& + J_m(kr_p) \sum_{n=0}^{\infty} [\tilde{A}_n^p (\alpha_{nm}^p \cos m\theta_p + \beta_{nm}^p \sin m\theta_p) + \tilde{B}_n^p (a_{nm}^p \cos m\theta_p + b_{nm}^p \sin m\theta_p)] \\
& + J_m(kr_p) \sum_{\substack{j=1 \\ \neq p}}^{N} \sum_{n=0}^{\infty} \tilde{A}_n^j [(C_{nm}^{jp} + \alpha_{nm}^{jp}) \cos m\theta_p + (D_{nm}^{jp} + \beta_{nm}^{jp}) \sin m\theta_p] \\
& \qquad + \tilde{B}_n^j [(E_{nm}^{jp} + a_{nm}^{jp}) \cos m\theta_p + (F_{nm}^{jp} + b_{nm}^{jp}) \sin m\theta_p] \Big\}.
\end{aligned} \tag{2.11}$$

Application of the body boundary condition now leads to the coupled systems of equations

$$\begin{aligned}
& I_p \epsilon_m \mathrm{e}^{\mathrm{i}m\pi/2} + A_m^p + \sum_{n=0}^{\infty} (\tilde{A}_n^p \alpha_{nm}^p + \tilde{B}_n^p a_{nm}^p) \\
& \quad + \sum_{\substack{j=1 \\ \neq p}}^{N} \sum_{n=0}^{\infty} [\tilde{A}_n^j (C_{nm}^{jp} + \alpha_{nm}^{jp}) + \tilde{B}_n^j (E_{nm}^{jp} + a_{nm}^{jp})] = 0,
\end{aligned} \tag{2.12}$$

and

$$B_m^p + \sum_{n=0}^{\infty} (\tilde{A}_n^p \beta_{nm}^p + \tilde{B}_n^p b_{nm}^p) + \sum_{\substack{j=1 \\ \neq p}}^{N} \sum_{n=0}^{\infty} [\tilde{A}_n^j (D_{nm}^{jp} + \beta_{nm}^{jp}) + \tilde{B}_n^j (F_{nm}^{jp} + b_{nm}^{jp})] = 0, \tag{2.13}$$

$p = 1, \ldots, N, m = 0, 1, \ldots$ in both cases. When $N = 1$ these equations are equivalent to those given in II, Section 4.

In order to evaluate the unknown complex coefficients A_n^j and B_n^j, the above infinite systems must be truncated. We in fact solve the systems

$$I_p \epsilon_m \, \mathrm{e}^{\mathrm{i}m\pi/2} + A_m^p + \sum_{n=0}^{M} (\tilde{A}_n^p \alpha_{nm}^p + \tilde{B}_n^p a_{nm}^p) + \sum_{\substack{j=1 \\ \neq p}}^{N} \sum_{n=0}^{M} [\tilde{A}_n^j (C_{nm}^{jp} + \alpha_{nm}^{jp}) + \tilde{B}_n^j (E_{nm}^{jp} + a_{nm}^{jp})] = 0, \tag{2.14}$$

and

$$B_m^p + \sum_{n=0}^{M} (\tilde{A}_n^p \beta_{nm}^p + \tilde{B}_n^p b_{nm}^p) + \sum_{\substack{j=1 \\ \neq p}}^{N} \sum_{n=0}^{M} [\tilde{A}_n^j (D_{nm}^{jp} + \beta_{nm}^{jp}) + \tilde{B}_n^j (F_{nm}^{jp} + b_{nm}^{jp})] = 0, \tag{2.15}$$

$p = 1, \ldots, N, m = 0, \ldots, M$ in both cases, as a single $N(2M+2) \times N(2M+2)$ system of linear algebraic equations.

The success of the multipole method depends on whether these equations can be solved accurately and efficiently. The value of the truncation parameter, M, required to achieve accurate results is therefore very important. It was found that a value of $M = 3$ was sufficient to give accuracy within 1% for most values of the geometrical and wave parameters. Most of the time used in solving the problem is spent setting up the coefficient matrix, in particular in evaluating the contour integrals in the definitions of $\alpha_{nm}^{jp}, \beta_{nm}^{jp}, a_{nm}^{jp}$ and $b_{nm}^{jp}, n, m = 0, \ldots, M, j, p = 1, \ldots, N$. For certain specific geometries computational time can be reduced by noting that these quantities are not all independent. For example, if considering a row of equally spaced cylinders on the channel centreline, we would have, from (A.10), $\alpha_{nm}^{j+1,j} = \alpha_{nm}^{j,j-1}, j = 2, \ldots, N-1$, with similar results for the other quantities.

We can now simplify the expression for ϕ by using the same idea as used in Linton and Evans [15]. If we substitute the equations (2.12) and (2.13) into the expression for ϕ, (2.11), and note the geometrical restriction on the use of Graf's addition theorem, it follows that, provided $r_p < R_{jp}, \forall_j$,

$$\phi(r_p, \theta_p) = \sum_{m=0}^{\infty} (Z_m^p H_m(kr_p) - J_m(kr_p))(A_m^p \cos m\theta_p + B_m^p \sin m\theta_p). \tag{2.16}$$

This expression provides an extremely simple formula for the velocity potential, and hence the free-surface elevation, in the vicinity of a cylinder. The potential on the cylinder surfaces has a particularly simple form. Using Wronskian relations for Bessel functions, we obtain

$$\phi(a_p, \theta_p) = -\frac{2\mathrm{i}}{\pi k a_p} \sum_{m=0}^{\infty} \frac{A_m^p \cos m\theta_p + B_m^p \sin m\theta_p}{H_m'(ka_p)}. \tag{2.17}$$

The first-order force on the jth cylinder is given by an integration of the pressure $(= \mathrm{i}\omega\phi)$ over the surface of the cylinder. The forces in the x and y directions are $\mathrm{Re}\{X^j \mathrm{e}^{-\mathrm{i}\omega t}\}$ and $\mathrm{Re}\{Y^j \mathrm{e}^{-\mathrm{i}\omega t}\}$, respectively, where

$$\begin{Bmatrix} X^j \\ Y^j \end{Bmatrix} = -\frac{\rho g A a_j \tanh kh}{k} \int_0^{2\pi} \phi(a_j, \theta_j) \begin{Bmatrix} \cos\theta_j \\ \sin\theta_j \end{Bmatrix} \mathrm{d}\theta_j \tag{2.18}$$

$$= \frac{2i\rho g A \tanh kh}{k^2 H_1'(ka_j)} \begin{Bmatrix} A_1^j \\ B_1^j \end{Bmatrix}. \tag{2.19}$$

It is convenient to non-dimensionalize these forces with respect to the force in the direction of wave advance on an isolated cylinder in the open sea as derived by MacCamy and Fuchs [17], $F^j = 4\rho g A \tanh kh/k^2 H_1'(ka_j)$. We obtain

$$\begin{Bmatrix} |X^j| \\ |Y^j| \end{Bmatrix} = \frac{1}{2}|F^j| \begin{Bmatrix} |A_1^j| \\ |B_1^j| \end{Bmatrix}. \tag{2.20}$$

The mean second-order drift force on the jth cylinder is given by the expression

$$f^j \equiv f_x^j + i f_y^j = \alpha_j \int_0^{2\pi} \left(\frac{1}{k^2}|\nabla\phi|^2 - |\phi|^2 \right)_{r_j = a_j} e^{i\theta_j} \, d\theta_j, \tag{2.21}$$

where $\alpha_j = \rho g A^2 a_j (1 + 2kh/\sinh 2kh)/8$, see for instance Kim and Yue [18]. The real and imaginary parts of f_j correspond to the drift force in the x and y directions, respectively. Note that these are steady forces, independent of time.

The drift force is most easily expressed in terms of the quantities

$$C_m^j = A_m^j - iB_m^j \quad \text{and} \quad D_m^j = A_m^j + iB_m^j. \tag{2.22}$$

We have, from (2.17),

$$\phi(a_j, \theta_j) = -\frac{i}{\pi k a_j} \sum_{m=0}^{\infty} \frac{C_m^j e^{-im\theta_j} + D_m^j e^{-im\theta_j}}{H_m'(ka_j)}, \tag{2.23}$$

and, from (2.16),

$$\nabla\phi(a_j, \theta_j) = \left(0, -\frac{i}{\pi k a_j^2} \sum_{m=1}^{\infty} \frac{m C_m^j e^{im\theta_j} - m D_m^j e^{-im\theta_j}}{H_m'(ka_j)} \right) \tag{2.24}$$

in polar coordinates. Substituting these expressions into (2.21), we obtain

$$f^j = \frac{2\alpha_j}{\pi (ka_j)^2} \left[-\frac{D_0^j \overline{C_1^j}}{H_0' \overline{H_1'}} - \frac{D_1^j \overline{C_0^j}}{H_1' \overline{H_0'}} + \sum_{n=1}^{\infty} \left(\frac{n(n+1)}{(ka_j)^2} - 1 \right) \left\{ \frac{C_n^j \overline{C_{n+1}^j}}{H_n' \overline{H_{n+1}'}} + \frac{\overline{D_n^j} D_{n+1}^j}{\overline{H_n'} H_{n+1}'} \right\} \right]. \tag{2.25}$$

In this expression all the Hankel functions have argument ka_j and an overbar denotes complex conjugate.

It is well known that when an incident wave is scattered by a body in a channel, the far field will consist of, apart from the incident wave itself, a finite sum of outgoing propagating modes, the form of which can be simply determined by means of separation of variables. Using the notation described in the Appendix, we can define reflection and transmission coefficients R_q and T_q by

$$\phi \sim \begin{cases} e^{ikx} + \sum_{q=0}^{\sigma} R_q \begin{Bmatrix} \cos q\pi y/2d \\ \sin q\pi y/2d \end{Bmatrix} e^{-ikxt_q} & x \to -\infty \\ \sum_{q=0}^{\sigma} T_q \begin{Bmatrix} \cos q\pi y/2d \\ \sin q\pi y/2d \end{Bmatrix} e^{ikxtq} & x \to \infty \end{cases}. \tag{2.26}$$

This definition seems more natural than that used in Butler and Thomas [9].

Hence, from (2.8) and (A.19)–(A.22) we obtain

$$R_q = \frac{\epsilon_q}{kdt_q}\sum_{j=1}^{N}\left[\begin{Bmatrix}\cos q\pi y_j/2d\\ \sin q\pi y_j/2d\end{Bmatrix}\sum_{n=0}^{\infty}(\tilde{A}^j_{2n}c_{2n}(t_q)+\mathrm{i}\tilde{A}^j_{2n+1}s_{2n+1}(t_q))\right.$$
$$\left.+\begin{Bmatrix}-\sin q\pi y_j/2d\\ \cos q\pi y_j/2d\end{Bmatrix}\sum_{n=0}^{\infty}(\mathrm{i}\tilde{B}^j_{2n}s_{2n}(t_q)+\tilde{B}^j_{2n+1}c_{2n+1}(t_q))\right]\mathrm{e}^{\mathrm{i}kx_jt_q} \tag{2.27}$$

and

$$T_q = \delta_{0q}+\frac{\epsilon_q}{kdt_q}\sum_{j=1}^{N}\left[\begin{Bmatrix}\cos q\pi y_j/2d\\ \sin q\pi y_j/2d\end{Bmatrix}\sum_{n=0}^{\infty}(\tilde{A}^j_{2n}c_{2n}(t_q)-\mathrm{i}\tilde{A}^j_{2n+1}s_{2n+1}(t_q))\right.$$
$$\left.+\begin{Bmatrix}-\sin q\pi y_j/2d\\ \cos q\pi y_j/2d\end{Bmatrix}\sum_{n=0}^{\infty}(-\mathrm{i}\tilde{B}^j_{2n}s_{2n}(t_q)+\tilde{B}^j_{2n+1}c_{2n+1}(t_q))\right]\mathrm{e}^{-\mathrm{i}kx_jt_q}. \tag{2.28}$$

In particular

$$R_0 = \frac{1}{kd}\sum_{j=1}^{N}\sum_{n=0}^{\infty}(-1)^n(\tilde{A}^j_{2n}+\mathrm{i}\tilde{A}^j_{2n+1})\mathrm{e}^{\mathrm{i}kx_j}, \tag{2.29}$$

and

$$T_0 = 1+\frac{1}{kd}\sum_{j=1}^{N}\sum_{n=0}^{\infty}(-1)^n(\tilde{A}^j_{2n}-\mathrm{i}\tilde{A}^j_{2n+1})\mathrm{e}^{-\mathrm{i}kx_j}. \tag{2.30}$$

The reflection and transmission coefficients are related by an equation representing the conservation of energy. This relation, together with others relating various hydrodynamic quantities of interest for channel problems, is derived in Linton and Evans [19]. In the notation of this paper we have

$$\sum_{q=0}^{\sigma}\frac{t_q}{\epsilon_q}(|R_q|^2+|T_q|^2)=1. \tag{2.31}$$

This identity was used as a check on all the numerical results that were obtained and was always satisfied to a high degree of accuracy. It should be noted that this does not by itself imply the accuracy of the results, but rather acts as a consistency check on the numerical implementation.

The far field can also be related to the total mean second-order drift force in the x direction. Such a formula was derived by Thomas [4] by considering the conservation of momentum flux down the channel. A more direct derivation can be obtained by applying Green's theorem to $\overline{\phi}$ and $\partial\phi/\partial x$ and this can be found in McIver and Linton [20]. The resulting identity is

$$\sum_{j=1}^{N}f_x^j = \frac{1}{2}\rho gA^2d\left(1+\frac{2kh}{\sinh 2kh}\right)\left(1+\sum_{q=0}^{\sigma}\frac{t_q^2}{\epsilon_q}(|R_q|^2-|T_q|^2)\right) \tag{2.32}$$

and this was also used as a check on the numerical accuracy of our results.

3. Small radius solution

In this section an approximate solution will be derived under the assumptions that the radii of all the cylinders are small relative to the wavelength of the incident wave, and that the wavelength and channel width are of the same order of magnitude. If we write a for the largest cylinder radius, then this is equivalent to $\epsilon \equiv ka \ll 1$, whilst $kd = O(1)$. A consequence of these assumptions is that the cylinder radius is much less than the channel width. We will also assume that the cylinders are not close to the channel walls, so that $|y_j| \ll d, j = 1, \ldots, N$. The method of solution is matched asymptotic expansions and follows closely that for the single cylinder case in II, Section 5.

For the inner region around cylinder j, extending to distances $r_j \ll k^{-1}$, scaled coordinates are defined by

$$\xi_j = \frac{x - x_j}{a}, \quad \eta_j = \frac{y - y_j}{a}, \quad \rho_j = \frac{r_j}{a}. \tag{3.1}$$

When written in terms of these coordinates, the inner potential $\psi(\xi_j, \eta_j) \equiv \phi(x, y)$ is seen to satisfy

$$\frac{\partial^2 \psi}{\partial \xi_j^2} + \frac{\partial^2 \psi}{\partial \eta_j^2} + \varepsilon^2 \psi = 0 \tag{3.2}$$

in the fluid region and the body boundary condition

$$\frac{\partial \psi}{\partial \rho_j} = -\frac{\partial \phi_I}{\partial \rho_j} = -\frac{\partial}{\partial \rho_j} \{e^{iX_j + i\varepsilon \xi_j}\} \quad \text{on } \rho_j = \widetilde{a_j}, \tag{3.3}$$

where $X_j = kx_j = O(1)$ and $\widetilde{a_j} = a_j/a$. Expanding the body boundary condition in powers of ε leads to

$$\frac{\partial \psi}{\partial \rho_j} = -I_j(i\varepsilon \cos\theta_j - \varepsilon^2 \widetilde{a_j} \cos^2\theta_j - \frac{1}{2} i\varepsilon^3 \widetilde{a_j}^2 \cos^3\theta_j + \cdots) \quad \text{on } \rho_j = \widetilde{a_j}, \tag{3.4}$$

where I_j is given by (2.6). The leading-order inner solution must satisfy the first approximations to (3.2) and (3.4) and is given by

$$\psi^{(1)} = i\varepsilon I_j \widetilde{a_j}^2 \frac{\cos\theta_j}{\rho_j}. \tag{3.5}$$

Here $\psi^{(\ell)}$ denotes the inner solution expanded to order ℓ in ε.

In the outer region, at distances $r_j \gg a, j = 1, \ldots, N$, scaled outer coordinates are defined by

$$X = kx, \quad Y = ky, \quad R_j = kr_j \tag{3.6}$$

and the outer solution $\Psi(X, Y) \equiv \psi(x, y)$ must satisfy all the conditions of the problem, except the body boundary condition. The outer solution will be constructed from the channel multipoles given in the Appendix, but now expressed in terms of the outer variables. When expressed in terms of the outer variables (3.5) gives

$$\psi^{(1,2)} = i\varepsilon^2 I_j \widetilde{a_j}^2 \frac{\cos\theta_j}{R_j}, \tag{3.7}$$

where $\psi^{(\ell,m)}$ denotes the inner solution to order ℓ in ε rewritten in terms of the outer variables and expanded to order m. A similar notation is used for the outer potential. Thus $\Psi^{(m)}$ denotes the order m outer solution which when rewritten in terms of the inner variables and expanded to order ℓ is denoted by $\Psi^{(m,\ell)}$. The matching principle then requires that $\psi^{(\ell,m)} \equiv \Psi^{(m,\ell)}$, see for example Crighton and Leppington [21].

The expansion (3.7) indicates that the leading-order outer solution is at $O(\varepsilon^2)$ and will contain terms no more singular than R_j^{-1}. Thus

$$\Psi^{(2)} = \varepsilon^2 \sum_{j=1}^{N} (A_0^j \phi_0^j + A_1^j \phi_1^j + B_1^j \psi_1^j) \tag{3.8}$$

where ϕ_m^j, ψ_m^j are channel multipoles and A_0^j, A_1^j, B_1^j are constants to be found from the matching. From (A.1) and (A.2), using the small argument expansions of the Bessel functions that are given by Abramowitz and Stegun ([16], p. 360), we understand that the leading-order terms in the inner expansion of (3.8) come from the dipole singularities at cylinder j. In particular

$$\Psi^{(2,1)} = \varepsilon^2 \left\{ A_1^p \left[\frac{2\cos\theta_p}{\pi \mathrm{i} \varepsilon \rho_p} \right] + B_I^p \left[\frac{2\sin\theta_p}{\pi \mathrm{i} \varepsilon \rho_p} \right] \right\} \tag{3.9}$$

so that matching with (3.7) gives

$$A_1^p = -\frac{1}{2}\pi I_p \widetilde{a_p}^2, \quad B_1^p = 0. \tag{3.10}$$

Using (A.1), (A.2), (A.14) and (A.15), we can show that the inner expansion of (3.8) about cylinder p continues as

$$\begin{aligned}
\Psi^{(2,3)} = \varepsilon^2 \Bigg\{ & A_0^p \left[1 + \frac{2\mathrm{i}}{\pi} \left(\log \frac{\varepsilon \rho_p}{2} + C \right) + \alpha_{00}^p + \frac{1}{2} \varepsilon \rho_p \beta_{01}^p \sin\theta_p \right] \\
& - \frac{1}{2}\pi I_p \widetilde{a_p}^2 \left[\frac{2}{\pi \mathrm{i} \varepsilon \rho_p} + \frac{\mathrm{i}}{\pi} \varepsilon \rho_p \log \varepsilon \rho_p \right. \\
& \qquad \left. + \frac{1}{2} \varepsilon \rho_p \left(1 - \frac{\mathrm{i}}{\pi}(1 - 2C + 2\log 2) + \alpha_{11}^p \right) \right] \cos\theta_p \\
& + \sum_{\substack{j=1 \\ \neq p}}^{N} \left[A_0^j \left(C_{00}^{jp} + \alpha_{00}^{jp} + \frac{1}{2} \varepsilon \rho_p ((C_{01}^{jp} + \alpha_{01}^{jp}) \cos\theta_p + (D_{01}^{jp} + \beta_{01}^{jp}) \sin\theta_p \right) \right. \\
& \left. - \frac{1}{2}\pi I_p \widetilde{a_j}^2 \left(C_{10}^{jp} + \alpha_{10}^{jp} + \frac{1}{2} \varepsilon \rho_p ((C_{11}^{jp} + \alpha_{11}^{jp}) \cos\theta_p + (D_{11}^{jp} + \beta_{11}^{jp}) \sin\theta_p \right) \right] \Bigg\}
\end{aligned} \tag{3.11}$$

where $C = 0.5772\ldots$ is Euler's constant. This expansion contains terms at orders ε, $\varepsilon^2 \log \varepsilon$, ε^2, $\varepsilon^3 \log \varepsilon$ and ε^3 which indicates the terms that need to be included in the order ε^3 inner solution. the procedure for determining this inner solution follows very closely that given in II, Section 5, for the single cylinder case; consequently only the result is given here, namely that

$$\psi^{(3)} = \mathrm{i} \varepsilon I_p \widetilde{a_p}^2 \frac{\cos\theta_p}{\rho_p} + Q_0 \varepsilon^2 \log \varepsilon + \varepsilon \left\{ Q_1 + \frac{1}{2} I_p \widetilde{a_p}^2 \left(\log \rho_p - \widetilde{a_p}^2 \frac{\cos 2\theta_p}{2\rho_p^2} \right) \right\}$$

$$+\varepsilon^3 \log\varepsilon \left\{ Q_2 + \left(\rho_p + \frac{\widetilde{a_p}^2}{\rho_p} \right) (Q_3 \cos\theta_p + Q_4 \sin\theta_p) \right\}$$
$$+\varepsilon^3 \left\{ -\frac{\mathrm{i}}{2} I_p \widetilde{a_p}^2 \left[\rho_p \log\rho_p \cos\theta_p + \frac{\widetilde{a_p}^4 \cos 3\theta_p}{12\rho_p^3} + \frac{\widetilde{a_p}^2 \cos\theta_p}{\rho_p} \left(\frac{7}{4} + \log\widetilde{a_p} \right) \right] \right.$$
$$\left. + Q_5 + \left(\rho_p + \frac{\widetilde{a_p}^2}{\rho_p} \right) (Q_6 \cos\theta_p + Q_7 \sin\theta_p) \right\} \tag{3.12}$$

where $Q_i, i = 0, \ldots, 7$, are constants to be determined. Expanding in the way described above, we have

$$\psi^{(3,2)} = \mathrm{i}\varepsilon I_p \widetilde{a_p}^2 \frac{\cos\theta_p}{\rho_p} + Q_0 \varepsilon^2 \log\varepsilon + \varepsilon^2 \left\{ Q_1 + \frac{1}{2} I_p \widetilde{a_p}^2 \log\rho_p \right\}$$
$$+\varepsilon^3 \log\varepsilon \{ Q_2 + \rho_p (Q_3 \cos\theta_p + Q_4 \sin\theta_p) \}$$
$$+\varepsilon^3 \left\{ -\frac{\mathrm{i}}{2} I_p \widetilde{a_p}^2 \rho_p \log\rho_p \cos\theta_p + \rho_p (Q_6 \cos\theta_p + Q_7 \sin\theta_p) \right\} \tag{3.13}$$

and then matching $\psi^{(3,2)}$ with $\Psi^{(2,3)}$ we obtain:

$$A_0^p = -\frac{\pi \mathrm{i}}{4} I_p \widetilde{a_p}^2, \tag{3.14}$$

$$Q_0 = \frac{2\mathrm{i}}{\pi} A_0^p, \tag{3.15}$$

$$Q_1 = A_0^p \left[1 + \frac{2\mathrm{i}}{\pi} (C - \log 2) + \alpha_{00}^p \right] + \sum_{\substack{j=1 \\ \neq p}}^{N} A_0^j [C_{00}^{jp} + \alpha_{00}^{jp} - 2\mathrm{i}(C_{10}^{jp} + \alpha_{10}^{jp})], \tag{3.16}$$

$$Q_2 = 0, \tag{3.17}$$

$$Q_3 = \frac{2}{\pi} A_0^p, \tag{3.18}$$

$$Q_4 = 0, \tag{3.19}$$

$$Q_6 = -\mathrm{i} A_0^p \left[1 - \frac{\mathrm{i}}{\pi} (1 - 2C + 2\log 2) + \alpha_{11}^p \right] + \sum_{\substack{j=1 \\ \neq p}}^{N} \frac{A_0^j}{2} [C_{01}^{jp} + \alpha_{01}^{jp} - 2\mathrm{i}(C_{11}^{jp} + \alpha_{11}^{jp})], \tag{3.20}$$

$$Q_7 = \frac{1}{2} A_0^p \beta_{01}^p + \sum_{\substack{j=1 \\ \neq p}}^{N} \frac{A_0^j}{2} [D_{01}^{jp} + \beta_{01}^{jp} - 2\mathrm{i}(D_{11}^{jp} + \beta_{11}^{jp})]. \tag{3.21}$$

Note that Q_5 is undetermined at this stage of the matching, but such constant terms in the inner potential do not contribute to the forces given below. On the other hand, they would contribute to higher-order forces such as the drift force on individual cylinders, so to this level of approximation nothing can be said about the effect of the channel on this drift force.

The first-order forces on the cylinders are given by (2.18). If we substitute from (3.12) and use the result

$$F^p \equiv \frac{4\rho g A \tanh kh}{k^2 H_1'(ka_p)} = \frac{4\rho g A \tanh kh}{k^2}\frac{\pi(ka_p)^2}{2\mathrm{i}}\left[1 - \frac{(ka_p)^2}{2}\log ka_p \right.$$
$$\left. - \frac{\pi(ka_p)^2}{4\mathrm{i}}\left(1 + \frac{\mathrm{i}}{\pi}(1 + 2C - 2\log 2)\right) + \cdots\right] \tag{3.22}$$

then we obtain the force ratios

$$\left|\frac{X^p}{F^p}\right| = \left|1 - \frac{\pi(ka_p)^2}{4\mathrm{i}}\alpha_{11}^p - \frac{\pi}{8}\sum_{\substack{j=1\\ \neq p}}^{N}\frac{I_j}{I_p}(ka_j)^2[C_{01}^{jp} + \alpha_{01}^{jp} - 2\mathrm{i}(C_{11}^{jp} + \alpha_{11}^{jp})]\right| \tag{3.23}$$

$$\left|\frac{Y^p}{F^p}\right| = \frac{\pi}{8}\left|(ka_p)^2\beta_{01}^p + \sum_{\substack{j=1\\ \neq p}}^{N}\frac{I_j}{I_p}(ka_j)^2[D_{01}^{jp} + \beta_{01}^{jp} - 2\mathrm{i}(D_{11}^{jp} + \beta_{11}^{jp})]\right|. \tag{3.24}$$

Methods for the efficient computation of the coefficients α_{nm}^{jp} and β_{nm}^{jp} are discussed in the Appendix.

4. Results

There are a large number of parameters in the problem and it will be helpful if we restrict our attention to some specific geometries. In an effort to study as realistic a situation as possible, we will only consider the case when all the cylinders have equal radius. Results for three different configurations are presented below. These correspond to two cylinders on the channel centreline, two cylinders placed symmetrically about the centreline and four cylinders arranged in a square, again symmetrically placed in the channel. In all cases the ratio a/d is fixed at 1/12 and the separation between the cylinder axes, s/d, is fixed at 1/2. The four-cylinder case then corresponds to that considered by Kashiwagi [11], though in his case the cylinders were truncated. The three geometries described above will be referred to as geometries 1, 2 and 3, respectively, and they are illustrated in Figure 2. The numbers in the figures are used in the text to refer to the individual cylinders. All the curves for forces and pressures are plotted against kd/π in the range $0 < kd/\pi < 4$ which is equivalent to $0 < ka \lesssim 1.05$ or $\infty > \lambda/a > 6$ where λ is the wavelength of the incident wave.

We begin with the simplest to calculate, and least affected by the channel walls, of the hydrodynamic quantities, namely the first-order forces given by (2.19). Results for first-order forces on arrays of two cylinders are given by Butler and Thomas [9, figures 4 and 6], but our computations suggest that these are in error.

Figure 3 shows the first-order force in the x-direction on both the front and back cylinders for geometry 1. The quantity plotted is the ratio of the force on the cylinder in the channel and the force that the cylinder would experience if the channel walls were absent. The latter was computed using the method described in Linton and Evans [15]. The effect of the channel appears to be greater for higher wavenumbers and this may be explained as due to the

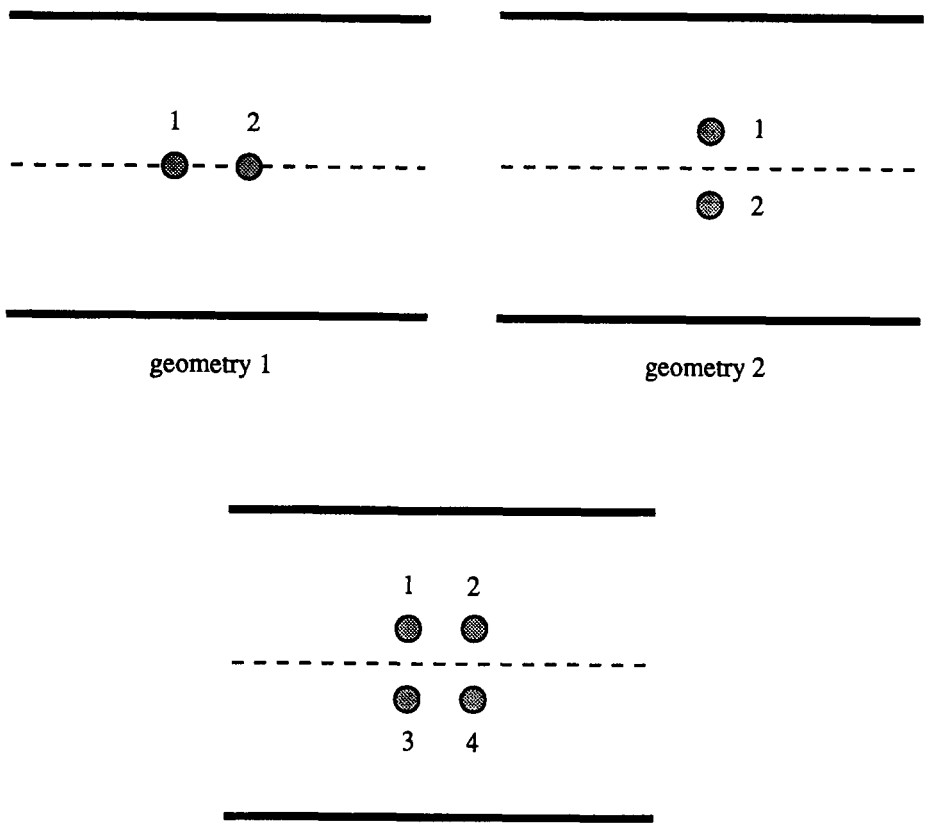

Figure 2. Sketch of the different geometries considered

increased influence of reflections from the channel walls at short wavelengths. The accuracy of the solution obtained using matched asymptotic expansions, given by (3.23), is shown in Figure 4 for the front cylinder in this case. The figure clearly demonstrates how the solution breaks down as the wavenumber increases, but the low wavenumber results give confidence in the results computed using the exact method.

For geometry 2 the first-order force ratios in the x-direction on the two cylinders are equal and do not differ from unity by more than 3% over the entire range of incident wavenumbers. For geometry 3 the forces on cylinders 3 and 4 are equal to those on cylinders 1 and 2, respectively, and these are shown in Figure 5. The behaviour is qualitatively similar to that shown in Figure 3. The cylinders are now off the channel centreline and this is the reason for the effect of the resonances at $kd = (2n-1)\pi/2$.

The relative effect of the channel walls on the first-order force in the y-direction is much more pronounced than on that in the x-direction, though the forces involved are much smaller. One example will suffice and this is provided by Figure 6 in which accurate and approximate solutions for the y-force on one of the front cylinders in geometry 3 is shown. It is clear that the channel resonances have an enormous effect on the force in the y-direction, particularly that at $kd = \pi$, where the resonance considerably affects the force over a wide range of wavenumbers around the resonance value. The approximate solution obtained from (3.24) is again very accurate for small kd, though it fails to pick up the abnormal behaviour at the antisymmetric cut-off values.

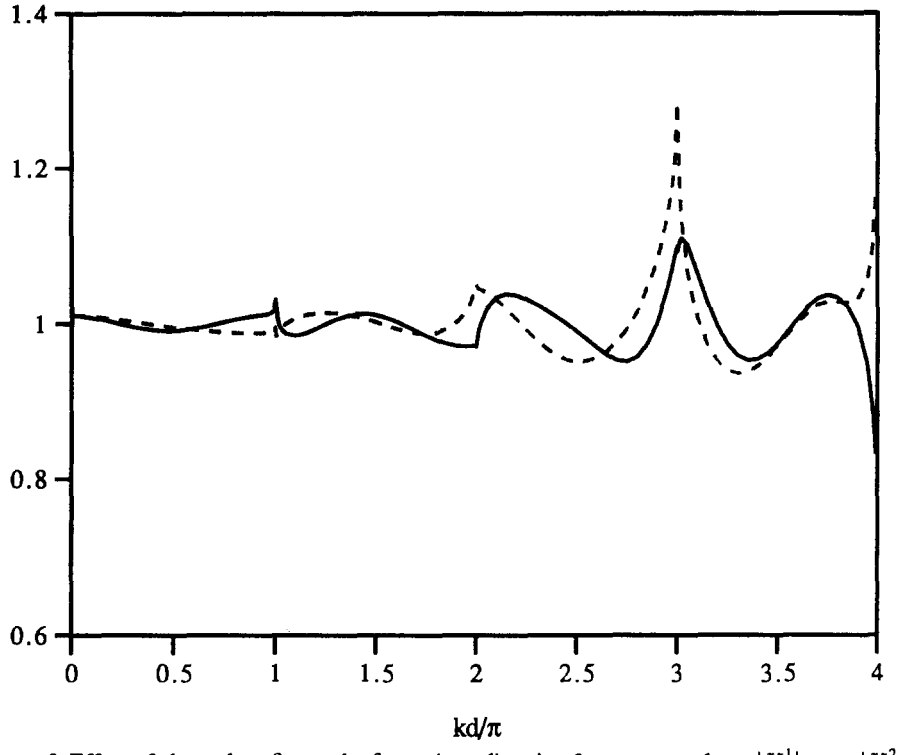

Figure 3. Effect of channel on first-order forces in x-direction for geometry 1. — $|X^1|$, --- $|X^2|$.

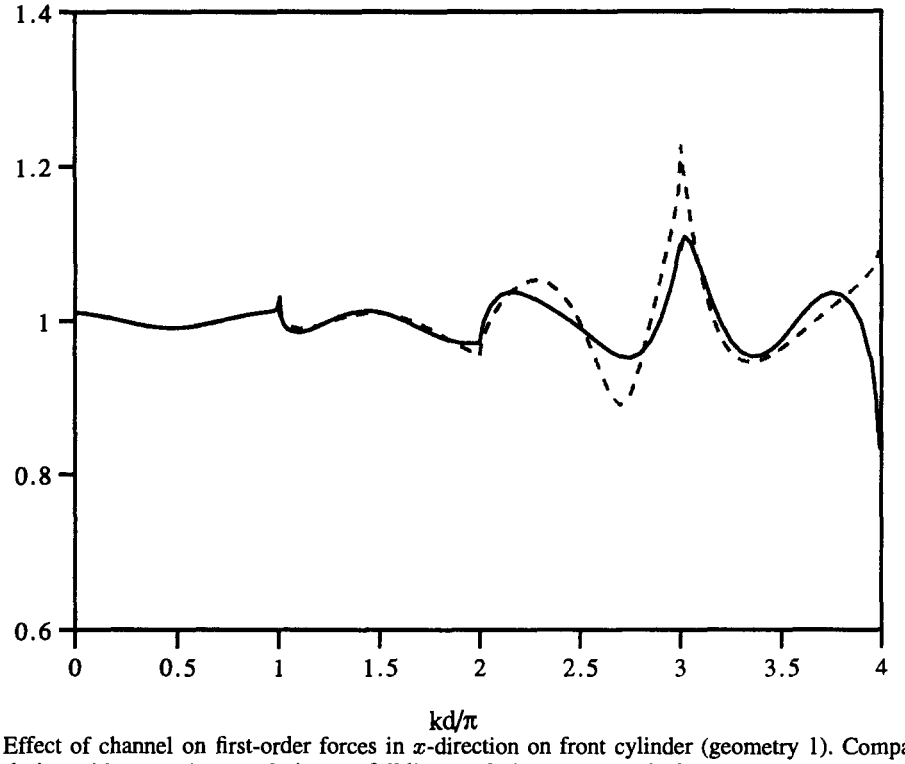

Figure 4. Effect of channel on first-order forces in x-direction on front cylinder (geometry 1). Comparison of accurate solution with approximate solution. — full linear solution, --- matched asymptotic expansions.

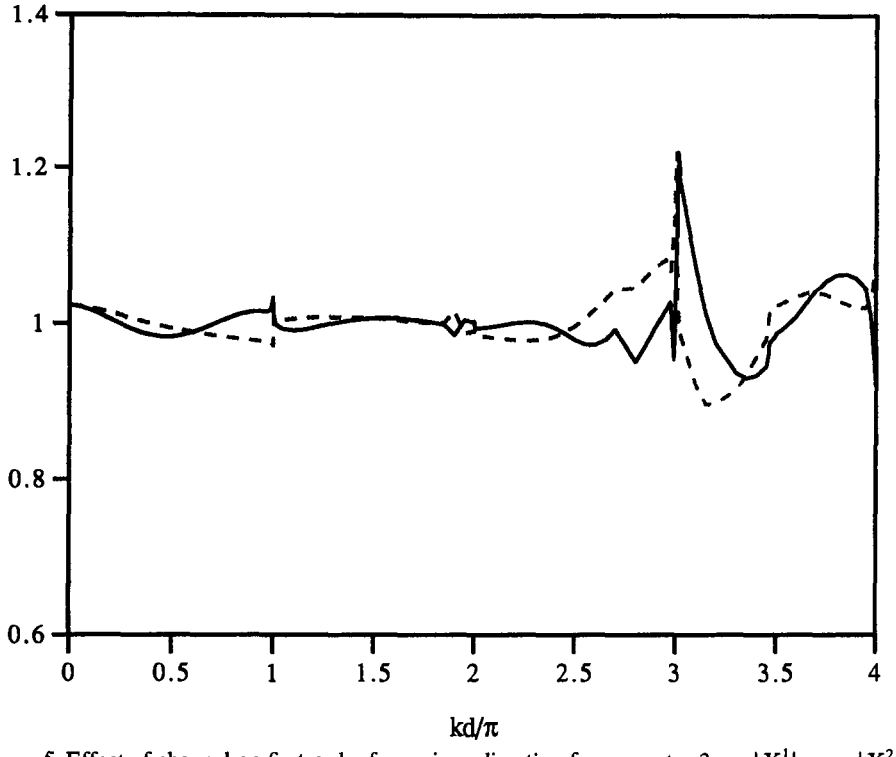

Figure 5. Effect of channel on first-order forces in x-direction for geometry 3. — $|X^1|$, --- $|X^2|$.

Both Thomas [4] and McIver [22] make the point that in the case of a single cylinder in a channel, the influence of the tank walls on the first-order force in the x-direction is significantly less than that on the actual pressures experienced on the cylinder surface. The pressure on the body is directly proportional to the potential ϕ which can be computed very simply from (2.17). Again we non-dimensionalize by dividing by the pressure that would be experienced if the cylinder array were in the open sea. Figure 7 shows the effect of the channel walls on the pressures around each cylinder for geometry 1 when the wavenumber is given by $ka = 0.4(kd/\pi \simeq 1.53)$. Owing to the symmetry of the geometry, the curves are plotted in the range $0 < \theta < \pi$, where $\theta = 0$ corresponds to the back of each cylinder and $\theta = \pi$ the front. The first-order force ratio at this wavenumber is seen from Fig. 3 to be very close to unity and thus these results are in accordance with previous studies.

In order to aid anyone trying to reproduce our numerical results, a list of values of the first-order force in the x-direction on cylinder 1 in geometries 1 and 3 is given in Table 1. Values are given for both the channel case and the open-sea case, each non-dimensionalized with respect to the force on a single cylinder in isolation. The curves shown in Figures 3 and 5 are ratios of these values.

A quantity of particular interest for the problem considered in this paper is the mean second-order drift force which can be computed via a near-field integration leading to (2.25) or, if only the total drift force in the x-direction is required, from the far-field reflection and transmission coefficients as in (2.32). This force, being steady rather than oscillatory in nature, is very important in the design of offshore structures. Extensive calculations of mean drift forces on arrays of cylinders in channel can be found in McIver and Linton [20]. A very simple and powerful approximate method for the determination of these second-order forces based

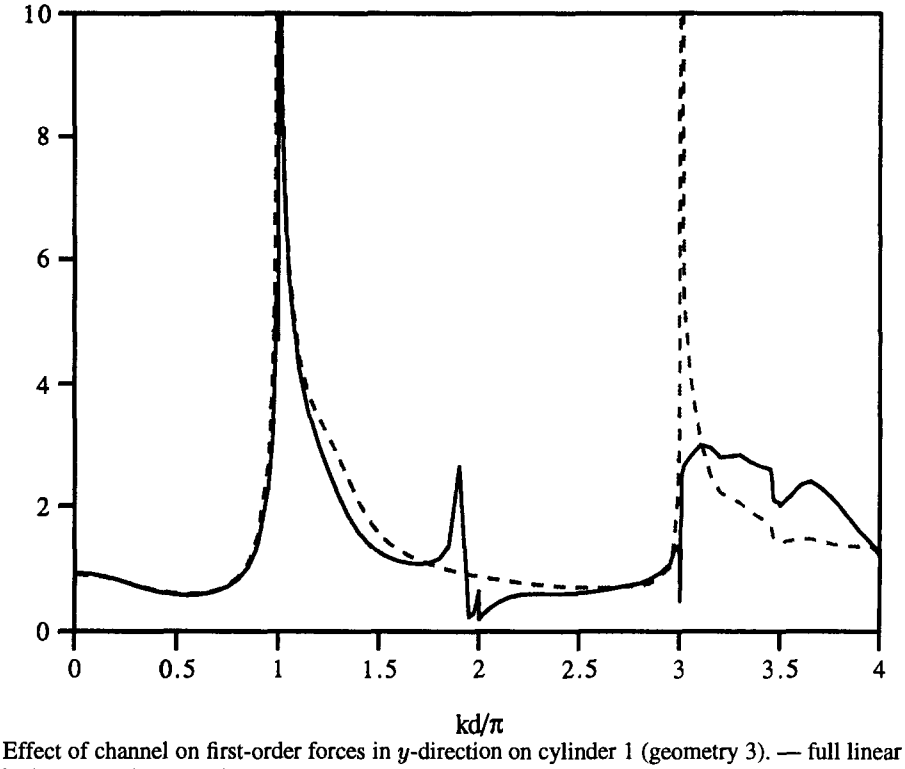

Figure 6. Effect of channel on first-order forces in y-direction on cylinder 1 (geometry 3). — full linear solution, --- matched asymptotic expansions.

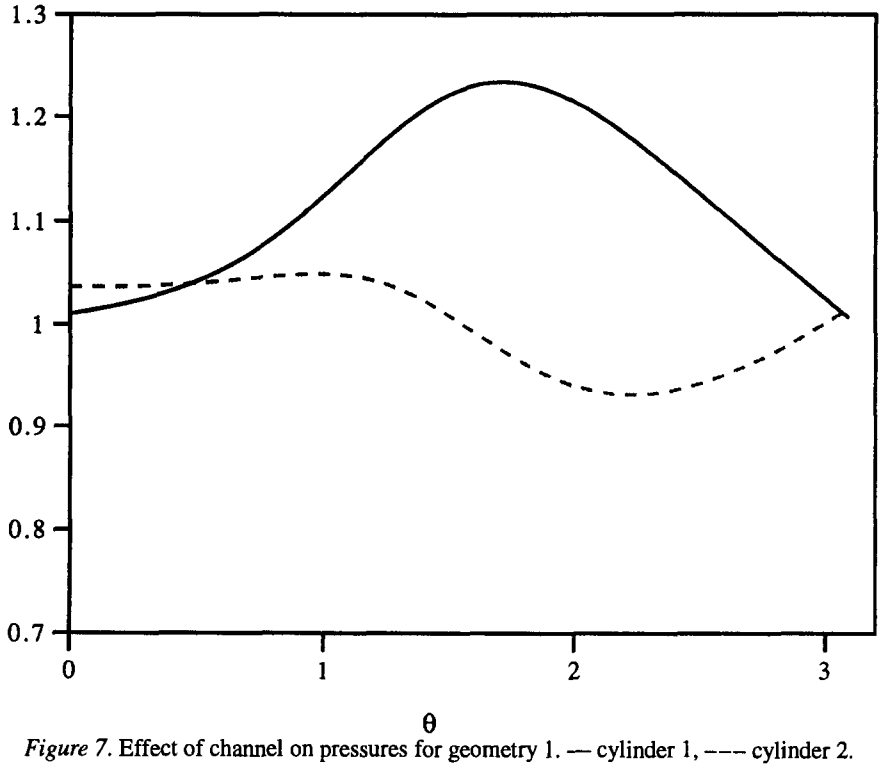

Figure 7. Effect of channel on pressures for geometry 1. — cylinder 1, --- cylinder 2.

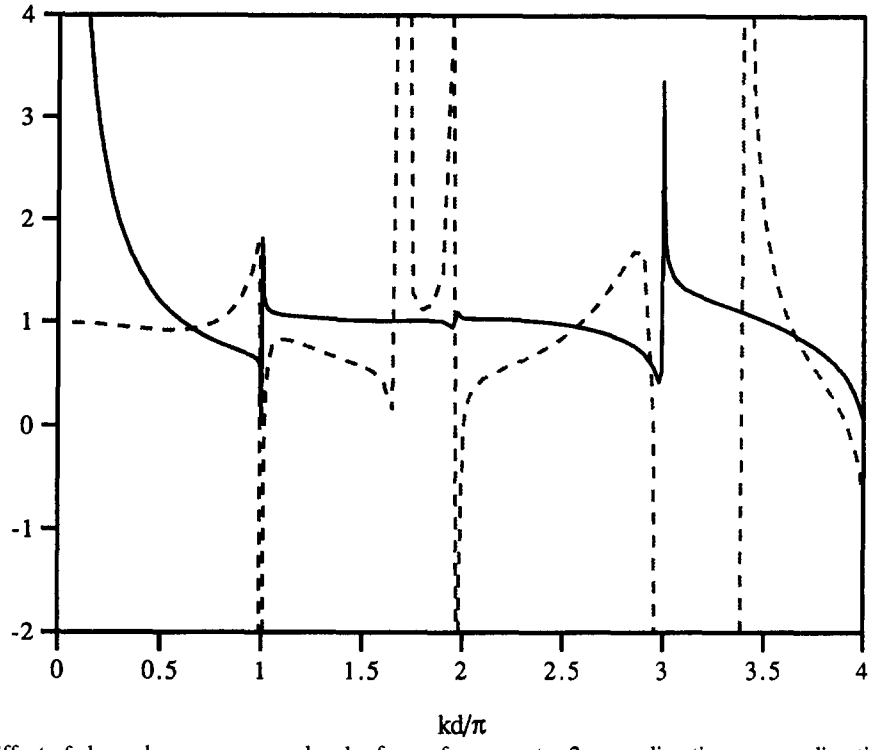

Figure 8. Effect of channel on mean second-order forces for geometry 2. — x-direction, ---- y-direction.

Table 1. First order forces on cylinder 1

	Geometry 1		Geometry 3	
kd/π	channel	open sea	channel	open sea
0.2	0.9746	0.9727	1.0071	1.0017
0.5	0.9501	0.9585	0.9579	0.9746
0.8	0.9552	0.9497	0.9641	0.9553
1.2	1.0418	1.0483	1.1150	1.1190
1.5	1.1828	1.1696	1.2130	1.2259
1.8	1.1592	1.1839	1.1307	1.1290
2.2	0.9939	0.9588	0.8152	0.8158
2.5	0.7516	0.7589	0.6422	0.6566
2.8	0.7192	0.7513	0.8605	0.8363
3.2	1.1023	1.1062	1.1774	1.2080
3.5	1.2804	1.3135	1.2231	1.2616
3.8	1.3178	1.2752	1.1790	1.1596

on the plane-wave approximation is also given there. Since publication of the above paper, a minor error in our numerical computations has come to light. The small spikes that occur at half-integer values of kd/π in Figures 4–9 of that paper are erroneous.

Here we shall indicate some typical behaviour by looking at results for geometry 2. Figure 8 shows both the x- and the y-force on cylinder 1 non-dimensionalized by the corresponding open-sea values. (The x-force on cylinder 2 is clearly the same as that for cylinder 1, whereas the y-force is equal and opposite.) A number of interesting features are apparent. Firstly, the

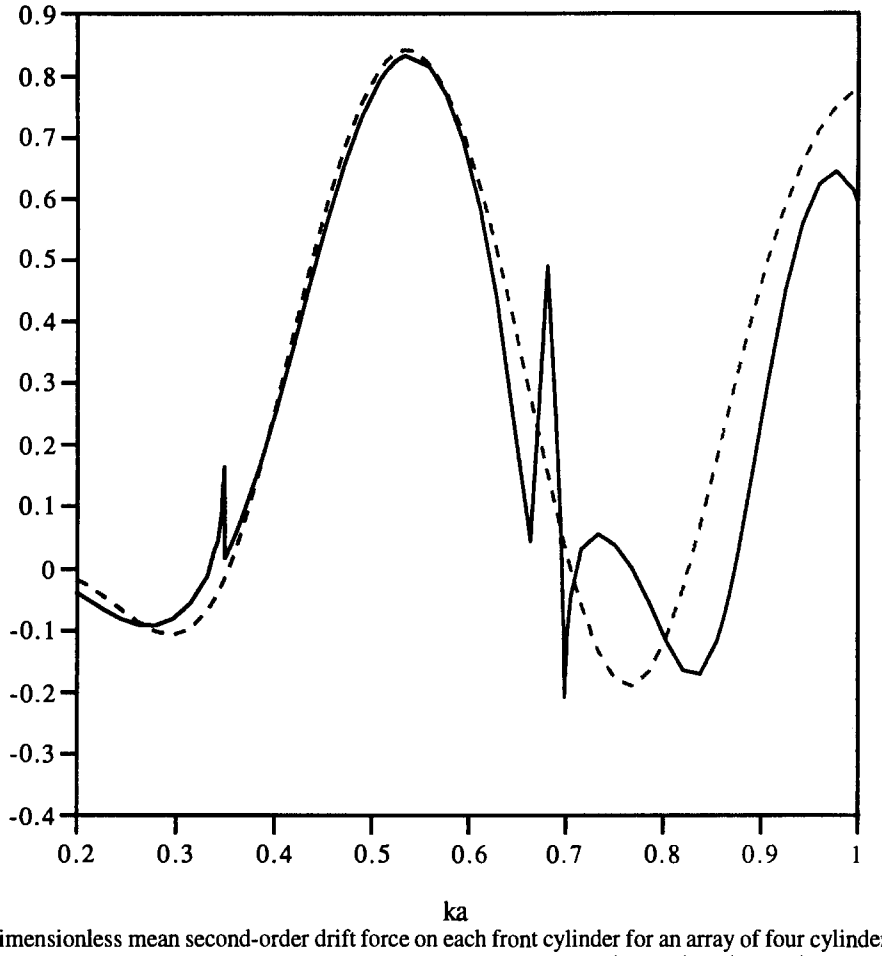

Figure 9. Dimensionless mean second-order drift force on each front cylinder for an array of four cylinders located symmetrically about the channel centreline in a square configuration with $a/d = 1/9$, $s/d = 1/6$ and $a/h = 0.1$. — open sea, --- channel.

behaviour in long waves of the x-direction force is fundamentally different to that of the cross-channel force. It should be noted that, although the x-direction force ratio gets very large as $ks \to 0$, the actual values of the drift force are very small. Secondly, we can see that as in the case of the first-order force, the effect on the y-force is significantly more than that on the x-force. For the x-force the force-ratio is quite close to unity for much of the graph, but the effects of the channel resonances is much larger than for the first-order forces. The curve for the y-force ratio is complicated by the fact that the open-sea drift force has two zeros in the range of wavenumbers plotted (at approximately $kd/\pi = 1.7$ and 3.4), which give rise to infinities in the force ratio plotted.

Results for the mean second-order drift force have been computed previously by Williams and Vazquez [12]. They plot graphs of the drift-force, non-dimensionalized by $\rho g a d h^2/4$ and Figure 9 may be directly compared with their Figure 12. Reference to their figure shows that over most of the frequency range the results are in very good agreement, though there are some discrepancies at and just above the cut-off value of $ka = 2\pi/9$.

Finally, we turn out attention to the far-field and compute reflection and transmission coefficients, using (2.27) and (2.28). Butler and Thomas [9] computed these coefficients for various two-cylinder arrays and our results have been checked with theirs, good agree-

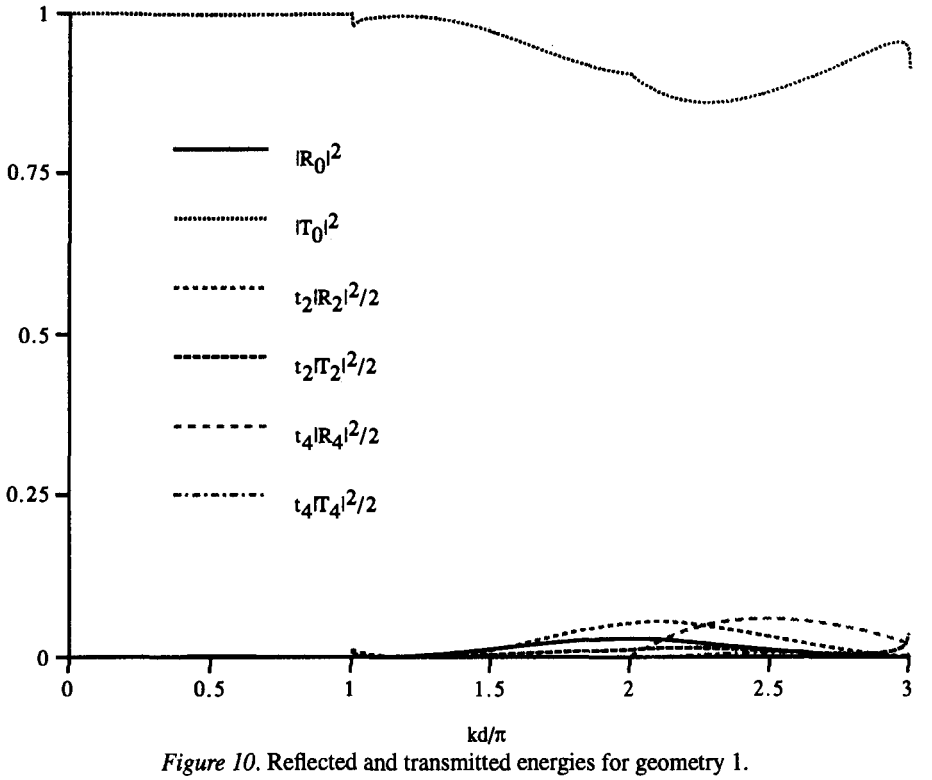

Figure 10. Reflected and transmitted energies for geometry 1.

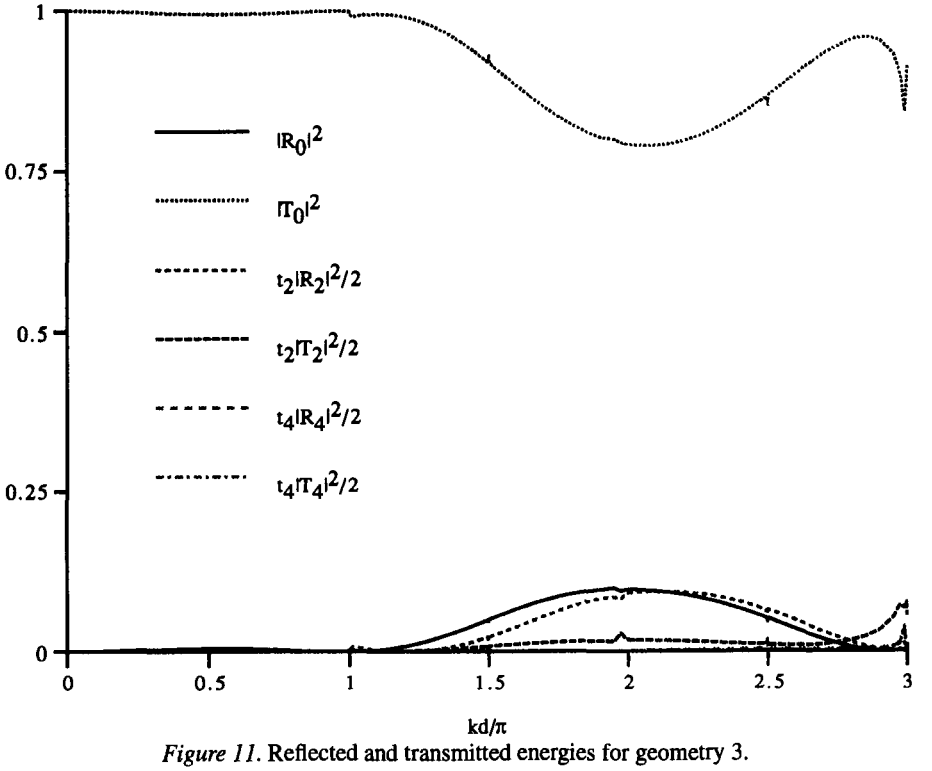

Figure 11. Reflected and transmitted energies for geometry 3.

ment being achieved. Perhaps the most useful quantity to plot is the energy associated with each reflected and transmitted propagating mode. Thus, from (2.31) we plot $t_q|R_q|^2/\epsilon_q$ and $t_q|T_q|^2/\epsilon_q, q = 0, \ldots, \sigma$. The curves in the figures then have the property that for any value of kd/π the values of the curves sum to unity. Another advantage of plotting the energy rather than the coefficients themselves is that it is easier to see that the energies (and hence the coefficients) are continuous across the cut-off frequencies. This problem is discussed in more detail in Linton and Evans [23].

In Figures 10 and 11 the reflected and transmitted energies are plotted over the range $0 < kd/\pi < 3$ for geometries 1 and 3. Owing to the symmetry of the geometries about the x-axis, $R_q = T_q = 0$ when q is odd. The cylinders in these examples are fairly small and not much energy is reflected back down the channel, particularly in long waves. Unsurprisingly, the four-cylinder array has more effect than the two-cylinder array.

5. Conclusion

The multipole method has been used to solve the full linear problem of the scattering of an incident plane wave in a channel by an arbitrary array of bottom-mounted vertical circular cylinders. This problem is of considerable practical importance from the point of view of performing model tests during the design of offshore structures.

A simple formula for the velocity potential on the surfaces of the cylinders has been derived which makes the computation of pressures and forces straightforward. The method also makes the evaluation of far-field quantities, such as the reflection and transmission coefficients, extremely simple. Extensive results for the various quantities of interest have been given.

An approximate solution to the problem, based on the assumption that the wavelength of the incident wave is long compared with the cylinder radii, has been derived, using matched asymptotic expansions. This leads to a simple method for calculating the first-order forces on the cylinders, which has been shown to be accurate when the non-dimensional wavenumber ka is less than about 0.5. This approximation is useful as a check on the results computed using the exact method.

Acknowledgement

CML gratefully acknowledges the support of the Nuffield Foundation.

Appendix A. Multipoles

Multipoles suitable for the problem under discussion have been constructed previously in II. Thus equations (3.19)–(3.24) of II can be written

$$\phi_n^j = H_n(kr_j)\cos n\theta_j + \sum_{m=0}^{\infty}(\alpha_{nm}^j \cos m\theta_j + \beta_{nm}^j \sin m\theta_j)J_m(kr_j), \tag{A.1}$$

$$\psi_n^j = H_n(kr_j)\sin n\theta_j + \sum_{m=0}^{\infty}(a_{nm}^j \cos m\theta_j + b_{nm}^j \sin m\theta_j)J_m(kr_j), \tag{A.2}$$

where

$$\alpha_{nm}^j = \frac{\epsilon_m \mathrm{i}^{n-m-1}}{\pi}\int_{-\infty}^{\infty}\frac{\mathrm{e}^{-2k\gamma d} + \cosh 2k\gamma y_j}{\gamma \sinh 2k\gamma d}\cosh m\tau \cosh n\tau \, \mathrm{d}t, \tag{A.3}$$

$$\beta_{nm}^j = \frac{2\mathrm{i}^{n-m}}{\pi} \int_{-\infty}^{\infty} \frac{\sinh 2k\gamma y_j}{\gamma \sinh 2k\gamma d} \sinh m\tau \cosh n\tau \, \mathrm{d}t, \tag{A.4}$$

$$a_{nm}^j = -\frac{\epsilon_m \mathrm{i}^{n-m}}{\pi} \int_{-\infty}^{\infty} \frac{\sinh 2k\gamma y_j}{\gamma \sinh 2k\gamma d} \cosh m\tau \sinh n\tau \, \mathrm{d}t, \tag{A.5}$$

$$b_{nm}^j = \frac{2\mathrm{i}^{n-m+1}}{\pi} \int_{-\infty}^{\infty} \frac{\mathrm{e}^{-2k\gamma d} - \cosh 2k\gamma y_j}{\gamma \sinh 2k\gamma d} \sinh m\tau \sinh n\tau \, \mathrm{d}t. \tag{A.6}$$

In these expressions τ is such that

$$\cosh \tau = t, \quad \sinh \tau = \gamma = \begin{cases} -\mathrm{i}(1-t^2)^{1/2} & t \le 1 \\ (t^2-1)^{1/2} & t > 1 \end{cases} \tag{A.7}$$

and the path of integration runs above the poles on the negative real axis and below those on the positive real axis. Note that if $m+n$ is odd $\alpha_{nm}^j = b_{nm}^j = 0$, whereas if $m+n$ is even $a_{nm}^j = \beta_{nm}^j = 0$. Also $\beta_{n0}^j = b_{n0}^j = 0$.

Techniques for numerically evaluating integrals of this type are discussed in I and II. In I, a method is described which consists of writing the contour integral as a sum of a principal-value integral plus the contribution from the finite number of poles on the real axis. A formula (Equation (2.61)) is then given which allows this principal-value integral to be easily computed. An alternative procedure is given in II. Here a change of variable is introduced which moves all the singularities onto the imaginary axis. The path of integration can then be deformed back into the real axis, leaving an integral of a well-behaved complex-valued function of a real variable which is straightforward to compute.

Formulas for multipoles singular at one point, (x_j, y_j), but expanded about another point, (x_p, y_p), can be obtained from integral representations for the multipoles (II, Equations (3.14) and (3.17)). We obtain, provided $j \neq p$,

$$\phi_n^j = H_n(kr_j)\cos n\theta_j + \sum_{m=0}^{\infty} (\alpha_{nm}^{jp} \cos m\theta_p + \beta_{nm}^{jp} \sin m\theta_p) J_m(kr_p), \tag{A.8}$$

$$\psi_n^j = H_n(kr_j)\sin n\theta_j + \sum_{m=0}^{\infty} (a_{nm}^{jp} \cos m\theta_p + b_{nm}^{jp} \sin m\theta_p) J_m(kr_p), \tag{A.9}$$

where

$$\alpha_{nm}^{jp} = \frac{\epsilon_m \mathrm{i}^{n-m-1}}{\pi} \int_{-\infty}^{\infty} \frac{\mathrm{e}^{-2k\gamma d}\cosh k\gamma(y_p - y_j) + \cosh k\gamma(y_p + y_j)}{\gamma \sinh 2k\gamma d} \mathrm{e}^{\mathrm{i}k(x_j - x_p)t} \cosh m\tau \cosh n\tau \, \mathrm{d}t, \tag{A.10}$$

$$\beta_{nm}^{jp} = \frac{2\mathrm{i}^{n-m}}{\pi} \int_{-\infty}^{\infty} \frac{\mathrm{e}^{-2k\gamma d}\sinh k\gamma(y_p - y_j) + \sinh k\gamma(y_p + y_j)}{\gamma \sinh 2k\gamma d} \mathrm{e}^{\mathrm{i}k(x_j - x_p)t} \sinh m\tau \cosh n\tau \, \mathrm{d}t, \tag{A.11}$$

$$a_{nm}^{jp} = \frac{\epsilon_m \mathrm{i}^{n-m}}{\pi} \int_{-\infty}^{\infty} \frac{\mathrm{e}^{-2k\gamma d}\sinh k\gamma(y_p - y_j) - \sinh k\gamma(y_p + y_j)}{\gamma \sinh 2k\gamma d} \mathrm{e}^{\mathrm{i}k(x_j - x_p)t} \cosh m\tau \sinh n\tau \, \mathrm{d}t, \tag{A.12}$$

$$b_{nm}^{jp} = \frac{\epsilon_m \mathrm{i}^{n-m+1}}{\pi} \int_{-\infty}^{\infty} \frac{\mathrm{e}^{-2k\gamma d}\cosh k\gamma(y_p - y_j) - \cosh k\gamma(y_p + y_j)}{\gamma \sinh 2k\gamma d} \mathrm{e}^{\mathrm{i}k(x_j - x_p)t} \sinh m\tau \sinh n\tau \, \mathrm{d}t. \tag{A.13}$$

Note that $\beta_{n0}^{jp} = b_{n0}^{jp} = 0$. We can expand the Hankel functions appearing in (A.8) and (A.9) in terms of (r_p, θ_p), using Graf's addition theorem, (Abramowitz and Stegun [16], Equation 9.1.79). We obtain

$$\phi_n^j = \sum_{m=0}^{\infty} [(C_{nm}^{jp} + \alpha_{nm}^{jp}) \cos m\theta_p + (D_{nm}^{jp} + \beta_{nm}^{jp}) \sin m\theta_p] J_m(kr_p), \quad j \neq p, \tag{A.14}$$

$$\psi_n^j = \sum_{m=0}^{\infty} [(E_{nm}^{jp} + a_{nm}^{jp}) \cos m\theta_p + (F_{nm}^{jp} + b_{nm}^{jp}) \sin m\theta_p] J_m(kr_p), \quad j \neq p, \tag{A.15}$$

where

$$C_{nm}^{jp} = \epsilon_m[(-1)^m H_{n+m}(kR_{jp}) \cos(m+n)\gamma_{jp} + H_{n-m}(kR_{jp}) \cos(m-n)\gamma_{jp}],$$

$$D_{nm}^{jp} = (-1)^m H_{n+m}(kR_{jp}) \sin(m+n)\gamma_{jp} + H_{n-m}(kR_{jp}) \sin(m-n)\gamma_{jp},$$

$$E_{nm}^{jp} = \epsilon_m[(-1)^m H_{n+m}(kR_{jp}) \sin(m+n)\gamma_{jp} + H_{n-m}(kR_{jp}) \sin(m-n)\gamma_{jp}]$$

and

$$F_{nm}^{jp} = -(-1)^m H_{n+m}(kR_{jp}) \cos(m+n)\gamma_{jp} + H_{n-m}(kR_{jp}) \cos(m-n)\gamma_{jp}.$$

The behaviour of ϕ_n^j, ψ_n^j as $|x| \to \infty$ can also be obtained from II, equations (3.14) and (3.17). We define

$$c_n(t) = \cos[n \sin^{-1} t], \quad s_n(t) = \sin[n \sin^{-1} t], \tag{A.16}$$

$$t_q = \left[1 - \left(\frac{q\pi}{2kd}\right)^2\right]^{1/2}, \quad q = 0, 1, \ldots, \sigma, \tag{A.17}$$

where σ is an integer such that

$$\sigma\pi < 2kd < (\sigma+1)\pi. \tag{A.18}$$

The following notation will be used. In bracketed pairs, if q is even, the upper element is meant, whereas if q is odd, the lower element is required. We then find that as $x \to \pm\infty$

$$\phi_{2n}^j \sim \sum_{q=0}^{\sigma} \frac{\epsilon_q c_{2n}(t_q)}{kdt_q} \begin{Bmatrix} \cos q\pi y_j/2d \\ \sin q\pi y_j/2d \end{Bmatrix} \begin{Bmatrix} \cos q\pi y/2d \\ \sin q\pi y/2d \end{Bmatrix} \mathrm{e}^{\pm \mathrm{i}k(x - x_j)t_q}, \tag{A.19}$$

$$\phi_{2n+1}^j \sim \mp \mathrm{i} \sum_{q=0}^{\sigma} \frac{\epsilon_q s_{2n+1}(t_q)}{kdt_q} \begin{Bmatrix} \cos q\pi y_j/2d \\ \sin q\pi y_j/2d \end{Bmatrix} \begin{Bmatrix} \cos q\pi y/2d \\ \sin q\pi y/2d \end{Bmatrix} \mathrm{e}^{\pm \mathrm{i}k(x - x_j)t_q}, \tag{A.20}$$

$$\psi_{2n}^j \sim \mp \mathrm{i} \sum_{q=1}^{\sigma} \frac{2s_{2n}(t_q)}{kdt_q} \begin{Bmatrix} -\sin q\pi y_j/2d \\ \cos q\pi y_j/2d \end{Bmatrix} \begin{Bmatrix} \cos q\pi y/2d \\ \sin q\pi y/2d \end{Bmatrix} \mathrm{e}^{\pm \mathrm{i}k(x - x_j)t_q}, \tag{A.21}$$

and

$$\psi^j_{2n+1} \sim \sum_{q=1}^{\sigma} \frac{2c_{2n+1}(t_q)}{kdt_q} \begin{Bmatrix} -\sin q\pi y_j/2d \\ \cos q\pi y_j/2d \end{Bmatrix} \begin{Bmatrix} \cos q\pi y/2d \\ \sin q\pi y/2d \end{Bmatrix} e^{\pm ik(x-x_j)t_q}. \tag{A.22}$$

References

1. R. Eatock Taylor and S.M. Hung, Mean drift forces on an articulated column oscillating in a wave tank. *Applied Ocean Research* 7 (2), (1985) 66–78.
2. R.W. Yeung and S.H. Sphaier, Wave-interference effects on a truncated cylinder in a channel. *J. Engrg. Math.* 23, (1989) 95–117.
3. R.W. Yeung and S.H. Sphaier, Wave-interference effects on a floating body in a towing tank. *Proc. PRADs '89*, Varna, Bulgaria (1989).
4. G.P. Thomas, The diffraction of water waves by a circular cylinder in a channel. *Ocean Engrg.* 18, (1991) 17–44.
5. C.M. Linton and D.V. Evans, The radiation and scattering of surface waves by a vertical circular cylinder in a channel. *Phil. Trans. R. Soc. Lond.* A 338, (1992) 325–357.
6. P. McIver and G.S. Bennett, Scattering of water waves by axisymmetric bodies in a channel. *J. Engrg. Math.* 27, (1993) 1–29.
7. M.A. Callan, C.M. Linton and D.V. Evans, Trapped modes in two-dimensional waveguides. *J. Fluid Mech.* 229, (1991) 51–64.
8. B.H. Bharatkumar, R. Mahadevan and M.R. Pranesh, Flume confinement effect on diffracted wave field around vertical cylinders. *Ocean Engrg.* 18, (1991) 521–533.
9. B.P. Butler and G.P. Thomas, The diffraction of water waves by an array of circular cylinders in a channel. *Ocean Engrg.* 20, (1993) 296–311.
10. S. Neelamani, B.H. Bharatkumar, R. Mahadevan and V. Sundar, Flume confinement effect on wave-induced dynamic pressures on twin-tandem cylinders. *Ocean Engrg.* 20, (1993) 313–337.
11. M. Kashiwagi, Radiation and diffraction forces acting on an offshore-structure model in a towing tank. *Intl Journal of Offshore and Polar Engrg.* 1, (1991) 101–107.
12. A.N. Williams and J.H. Vazquez, Mean drift loads on array of vertical cylinders in narrow tank. *Journal of Waterway, Port, Coastal, and Ocean Engineering* 119 (4), (1993) 398–416.
13. C.M. Linton, On the free-surface Green's function for channel problems. *Applied Ocean Research* 15, (1993) 263–267.
14. C.M. Linton and D.V. Evans, Integral equations for a class of problems concerning obstacles in waveguides. *J. Fluid Mech.* 245, (1992) 349–365.
15. C.M. Linton and D.V. Evans, The interaction of waves with arrays of vertical circular cylinders. *J. Fluid Mech.* 215, (1990) 549–569.
16. M. Abramowitz and I.A. Stegun, *Handbook of Mathematical Functions*, New York: Dover (1965).
17. R.C. MacCamy and R.A. Fuchs, Wave forces on piles: A diffraction theory. US Army Costal Engineering Research Center. *Tech. Mem.* 69 (1954).
18. M.-H. Kim and D.K.P. Yue, The complete second-order diffraction solution for an axisymmetric body. Part 1. Monochromatic incident waves. *J. Fluid Mech.* 200, (1989) 235–264.
19. C.M. Linton and D.V. Evans, Hydrodynamic characteristics of bodies in channels. *J. Fluid Mech.* 252, (1993) 647–666.
20. P. McIver and C.M. Linton, Mean drift forces on arrays of axisymmetric structures in a wave tank. *Applied Ocean Research* 16, (1994) 327–335.
21. D.G. Crighton and F.G. Leppington, Singular perturbation methods in acoustics: diffraction by a plate of finite thickness. *Proc. R. Soc. Lond.* A 335, (1973) 313–339.
22. P. McIver, The wave field scattered by a vertical cylinder in a narrow wave tank. *Applied Ocean Research* 15, (1993) 25–37.
23. C.M. Linton and D.V. Evans, The interaction of waves with a row of circular cylinders. *J. Fluid Mech.* 251, (1993) 687–708.